energy&fuels

Article

Cite This: Energy Fuels 2017, 31, 12120-12132

pubs.acs.org/EF

A Compact Kinetic Model for Biomass Pyrolysis at Gasification Conditions

Himanshu Goyal[†] and Perrine Pepiot*[,‡]

[†]Robert F. Smith School of Chemical and Biomolecular Engineering, Cornell University, Ithaca, New York 14853, United States

[‡]Sibley School of Mechanical and Aerospace Engineering, Cornell University, Ithaca, New York 14853, United States

Supporting Information

ABSTRACT: Computational fluid dynamics (CFD) tools are increasingly gaining importance to obtain detailed insight into biomass gasification. A major shortcoming of the current CFD tools to study biomass gasification is the lack of computationally affordable chemical kinetic models, which allows detailed predictions of the yield and composition of various gas and tar species in complex reactor configurations. In this work, a detailed mechanism is assembled from the literature and reduced to a compact model describing the gas-phase reactions of biomass gasification in the absence of oxygen. The reduction procedure uses a graph-based method for unimportant kinetic pathways elimination and quasi-steady-state species selection. The resulting reduced model contains 39 gas species and 118 reactions and is validated against the detailed model and two experimental configurations: the pyrolysis of volatile species, such as levoglucosan, in a tubular reactor, and the fast pyrolysis of biomass particles in a drop tube reactor. The reduced model predicts the evolution of major gas products (e.g., CO, CO_2, CH_4, H_2) and various classes of tar (e.g., single-ring aromatics, oxygenated aromatics, PAHs) produced during biomass gasification. The capability of the reduced model to adequately capture the chemical process in a complex reactor geometry at an acceptable computational cost is demonstrated by employing it in a simulation of a pseudo two-dimensional laboratory-scale fluidized bed reactor.

1. INTRODUCTION

Biomass (e.g., wood, energy crops, agricultural residue, municipal waste, etc.) is recognized as an essential renewable source of energy that can help in reducing the current dependence on fossil fuels. Thermochemical conversion in fluidized bed reactors (FBRs) is a promising technology to convert low-value lignocellulosic biomass into high energy density gaseous or liquid fuel. This process utilizes heat and/or physical catalysts to convert biomass to an intermediate gas or liquid, followed by an additional conversion step to transform that gas or liquid into a biofuel. It has the ability to robustly handle a wide range of feedstock and to produce both liquid and gaseous fuels.

Thermochemical conversion of biomass can be divided into two major classes: pyrolysis and gasification. Pyrolysis is performed at relatively low temperatures (773−872 K) maximizing the yield of liquid fuel, whereas gasification is performed at higher temperatures (1073−1273 K) maximizing the yield of gaseous fuel. In this work, we focus on the latter, namely, biomass gasification. One of the major challenges in making biomass gasification an economically viable technology is the reduction or elimination of tars, which are complex mixtures of condensable hydrocarbons.[1,2] Different tar species exhibit different properties, for example, heterocyclic compounds (e.g., phenol) exhibit high water solubility, whereas polycyclic aromatic hydrocarbons (PAH) can condense at relatively high temperatures.[2] On the basis of its composition, tar can condense in downstream equipment, causing fouling or plugging, and can also produce hazardous tar−water mixtures,[2] and therefore needs to be removed. At present, design and scale-up of FBR for biomass gasification are mostly empirically based, relying heavily on expensive and lengthy pilot-scale reactor studies. Yet, measurements in these reactors are unlikely to be detailed enough to improve our understanding of tar formation processes for various operating conditions and feedstock, necessary to efficiently optimize the conversion process.[3] Mathematical modeling and simulation tools provide a much more flexible and affordable framework to investigate the controlling chemical and physical processes, with the potential to play a determining role in the development and deployment of the technology.

While the field has seen recent major advances, further improvements are still required, especially in the description of chemical processes, before numerical tools can be utilized to their full potential. Gomez-Barea et al.,[4] in their review paper, recognize a strong need for modeling efforts in biomass devolatilization and tar chemistry. However, the chemistry of this conversion process is extremely complicated to model due to the high variability of the feedstock, the complex structure of biomass particles, as well as the interaction between chemistry and the multiphase flow dynamics typically found in gasification reactors.[5] These difficulties have hindered the development of detailed kinetic models for biomass thermochemical conversion chemistry and have entailed the use of detailed mechanisms for combustion and pyrolysis of various hydrocarbon species, developed in the combustion literature, to represent biomass gasification. For instance, Debiagi et al.[5] and Norinaga et al.[6] have developed detailed kinetic models for thermochemical conversion of biomass starting from the kinetic models for various hydrocarbons available in the combustion literature.

Received: June 8, 2017
Revised: September 28, 2017
Published: October 2, 2017

DOI: 10.1021/acs.energyfuels.7b01634
Energy Fuels 2017, 31, 12120−12132

However, the resulting detailed mechanisms consist of a large number of elementary and nonelementary reactions ($O(10^4)$) and chemical species ($O(10^3)$), making them computationally unaffordable to use in CFD simulations. These detailed mechanisms are thus more suitable for zero-dimensional configurations neglecting the transport processes. In the absence of a computationally affordable chemical mechanism, most of the existing modeling studies of biomass thermochemical conversion either neglect the gas-phase reactions[7−9] or use very simple kinetic models.[10−21] These kinetic models describe biomass devolatilization and evolution of gas-phase primary products using a few model compounds and global reactions, whose rates are fitted using available experimental data, such as Thermogravimetric Analysis (TGA). While these global models can be fitted *a priori* to provide trends in terms of the major controlling parameters, such as reactor operating temperature, they are not appropriate whenever more quantitative or detailed information is sought from CFD calculations. For instance, these models cannot be used to understand how tertiary tars are created in highly unsteady multiphase flows. An intermediate level of chemical detail is then desirable that can provide refined predictions in simulations, while remaining computationally affordable. The goal of this paper is to develop such a model for biomass gasification. Note that we will focus on the initial volatile release and subsequent gas-phase evolution in the absence of oxygen, the resulting model requiring to be complemented by a kinetic model to fully describe the long-term heterogeneous reactions of gasification.

Several automated kinetic reduction techniques have been developed in the combustion community. In general, these reduction techniques analyze a detailed mechanism for a given set of conditions to predict the redundant species and reactions and remove them from the chemical mechanism. Recently, Løvås et al.[22] used a combined reaction flow and sensitivity analysis to develop a compact mechanism for gas-phase reactions of biomass combustion. This mechanism was developed in a homogeneous reactor configuration for a fixed inlet gas composition and variable temperature.

In this work, we focus on the secondary gas-phase reactions occurring at gasification conditions and compile a detailed mechanism from the literature describing those reactions. We then use the DRGEP (Direct Relation Graph with Error Propagation) technique[23] to extract a reduced model from the detailed one. The reduction procedure accounts for the variability in the primary products expected to be found in gasification reactors by using a statistical Partially Stirred Reactor (PaSR) configuration. Coupled with an appropriate biomass devolatilization model (here, the work of Corbetta et al.,[24] as described below), the resulting reduced model describes the secondary gas-phase reactions of biomass devolatilization products in a pure nitrogen environment at temperatures relevant for gasification (1073−1273 K). Note that partial oxidation and steam reforming are not included in this study.

The remainder of this paper is organized as follows: Section 2 describes how the reference chemical kinetic model for the gas-phase chemistry and biomass devolatilization chemistry are assembled from the literature. In Section 3, the automatic reduction procedure used to generate a compact model that accurately reproduces the dynamics of the detailed model is presented. Validation is detailed in Section 4. Finally, in Section 5, the applicability of the reduced model in complex CFD configurations is demonstrated by simulating a pseudo two-dimensional laboratory-scale FBR.

2. REFERENCE DETAILED CHEMICAL KINETIC MODEL

A description of the reference detailed chemical models for the solid biomass devolatilization and the subsequent secondary gas-phase reactions of the primary devolatilization products is first provided.

2.1. Biomass Devolatilization Model. The high variability of feedstock and the structural complexity of biomass particles prevent the development of detailed kinetic models for describing the transition of the solid biomass into gas and char during devolatilization. In the absence of a more detailed description of the biomass devolatilization, the lumped chemical model developed by the CRECK modeling group[24] is used here to describe the first step of biomass gasification, i.e., devolatilization. This model consists of 24 reactions involving 12 solid species, 7 trapped gases slowly releasing from the solid matrix, and 20 gas-phase products. The initial composition of biomass is represented by a combination of cellulose, hemicellulose, and 3 types of lignin. The rates of the lumped reactions are fitted to match a series of thermogravimetric weight loss experiments. It is worth noting that these reactions are irreversible, implying that the gas composition surrounding the particle does not affect the chemistry going on at the particle level. This model has been validated against a series of experiments for various operating conditions and feedstock.[24−26]

2.2. Primary Product Decomposition and Tar Formation. The biomass devolatilization model creates a variety of gas-phase species, called primary products, whose evolution in the gas phase at gasification temperature must be modeled. These molecules usually are high molecular weight heterogeneous species, such as levoglucosan or phenolic compounds. Some of these molecules, often found in combustion systems (e.g., phenol), have been extensively studied, and accurate mechanisms for their decomposition to small hydrocarbons are available. Recently, we have developed and extensively validated a kinetic model for hydrocarbon pyrolysis and oxidation for combustion applications, the latest version containing a large selection of alkanes up to dodecane and aromatic species, such as phenol, toluene, benzene, xylene, and two-ringed aromatics (e.g., α-methylnaphthalene).[27−32] In the combustion process, ethylene is placed at the center of molecular growth, and we assume that the same holds true for the tars growth in biomass pyrolysis and gasification. To assemble the detailed model, we combine several chemical modules independent from one another, namely, a biomass devolatilization model to form primary products from solid biomass, a primary product decomposition model, and a detailed scheme for polycyclic aromatic hydrocarbon formation. A few of the primary gas-phase species produced by devolatilizing biomass are quite specific to the biomass constitutive components, and have not received the same amount of characterization as typical combustion molecules. To describe their decomposition, the lumped chemical reactions available from Calonaci et al.[26] are used. They include levoglucosan, 5-hydroxymethyl furfural, hydroxyacetaldehyde, xylose, coumaryl, and their direct decomposition products (see the Supporting Information document for more details). In the pyrolysis conditions of relevance here, the unimolecular decomposition reactions of those compounds are controlling their overall decomposition rates, as they are responsible for creating the initial radical pool.

DOI: 10.1021/acs.energyfuels.7b01634
Energy Fuels 2017, 31, 12120−12132

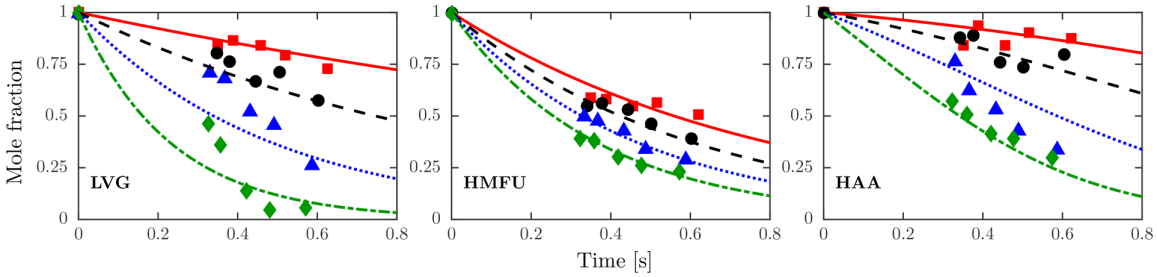

Figure 1. Pyrolytic decomposition of levoglucosan (LVG), hydroxyacetaldehyde (HAA), and 5-hydroxymethyl furfural (HMF): Comparison between simulation results using the reference chemical model (lines) and experiments (Shin et al.,[33] symbols). Different symbols indicate different temperatures (square: 898 K, circle: 923 K, triangle: 948 K, and diamond: 973 K).

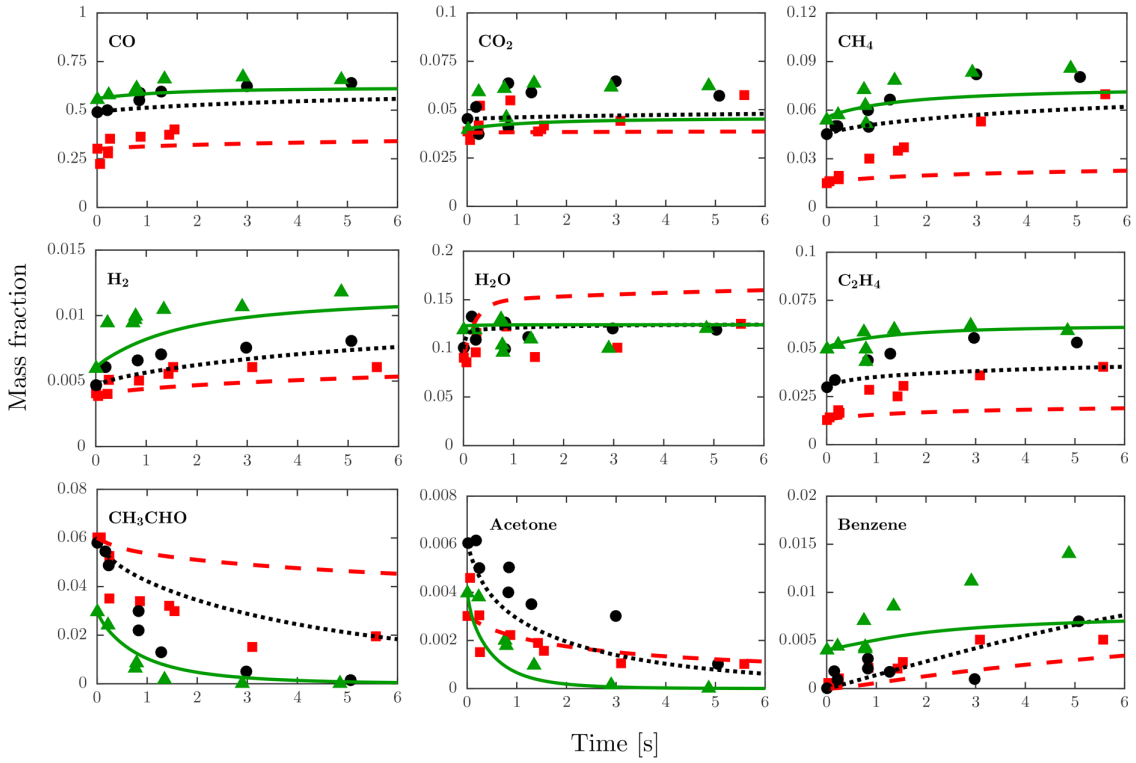

Figure 2. Pyrolytic decomposition of major cellulose devolatilization products: Comparison between simulation results using the reference chemical model (lines) and experiments (Norinaga et al.,[6] symbols). Different symbols indicate different temperatures (square: 973 K, circle: 1023 K, and triangle: 1073 K).

The chemical mechanism on which those reactions are added being different from the one they have been developed for, especially in terms of the small radicals chemistry, we found that it was necessary to adjust slightly the unimolecular decomposition rates for levoglucosan, 5-hydroxymethyl furfural, and hydroxyacetaldehyde to properly capture the rates experimentally measured by Shin et al.[33] In those cases, the rates proposed by Shin et al.[33] were in general adopted, staying as close to the branching ratios of Calonaci et al.[26] as possible whenever competing reactions were involved. One exception is for hydroxyacetaldehyde, for which Calonaci et al. and Shin et al.[33] decomposition pathways were combined and manually adjusted to reflect the added pathways.

The detailed model consists of 396 molecular species and 3210 elementary reaction steps and is validated against the experiments by Shin et al.[33] in Figure 1, and Norinaga et al.[6] in Figure 2. Shin et al.[33] studied the pyrolysis of levoglucosan (LVG), 5-hydroxymethyl furfural (HMF), and hydroxyacetaldehyde (HAA) in a flow tube reactor for temperatures ranging from 773 to 1023 K. Norinaga et al.[6] studied the secondary pyrolysis of nascent volatiles generated from the fast pyrolysis of cellulose in a tubular reactor in the temperature range of 973−1073 K. Assuming that there is no significant axial mixing in the tubular reactors of both experiments, these reactors are modeled as zero-dimensional isobar homogeneous systems. As can be seen from Figures 1 and 2, simulation results show very good agreement with the experiments, especially considering the high uncertainty on initial conditions that sometimes exist in the pyrolysis experiments. Additional validation cases considering the evolution of phenolic and aromatics compounds can be found in the Supporting Information document.

DOI: 10.1021/acs.energyfuels.7b01634
Energy Fuels 2017, 31, 12120−12132

3. REDUCED CHEMICAL MODEL DEVELOPMENT

The reference kinetic model for the gas-phase reactions described in the previous section is too complex to be used even in simple CFD configurations. Therefore, the objective is to identify the most important chemical reaction pathways for gasification. This section describes how this objective is achieved by extracting a compact model with 39 species and 118 reactions from the reference model with 396 species and 3210 reactions. Note that the reduction process does not affect the solid-to-gas devolatilization model[24] in any way.

3.1. Relevant Gasification Conditions. As all reactions are not important at all conditions, the very first task is to identify the conditions at which gasification will most likely take place in an actual gasifier, in particular, the heating rate to which biomass will be subjected. This step will help refine the range of conditions over which the reduced chemical kinetic model should be valid, and focus the reduction procedure on the relevant kinetics. Table 1 shows the parameters used to represent the devolatilization of biomass particles in an FBR. The size of biomass particles varies between 300 μm and 1 mm to represent the general size range found in many laboratory gasification studies. Gas-phase properties, such as density, specific heat capacity, conductivity, and viscosity, are computed assuming pure nitrogen at the temperatures and pressure stated in Table 1. To estimate typical heating rates, the Nusselt correlation from Gunn[34] is used along with the parameters from Table 1. For these parameters, Biot numbers for the biomass particles vary between 0.34 and 0.58, implying that thermal gradients will be present in the biomass particles. However, the purpose of Table 1 is to establish relevant conditions in order to apply our chemistry reduction algorithms. For this, an assumption of constant internal temperature suffices. Simulations of biomass devolatilization using the Corbetta et al. model,[24] and neglecting secondary gas-phase reactions, show that most primary gases are released from the biomass between 773 and 873 K. With this assumption, Figure 3 indicates that particles of size between 300 μm and 1 mm experience a heating rate of $O(10^3)$ K/s during devolatilization. Therefore, a value of 1000 K/s is chosen as representative of the heating rate for the reduction procedure.

Table 1. Parameters Used To Estimate Relevant Biomass Particle Heating Rates for the Chemistry Reduction Procedure

parameter	value
gas temperature	1073−1273 K
particle temperature during devolatilization	773−873 K
pressure	1 atm
solid heat capacity	2300 J/kg·K
biomass bulk density	650 kg/m^3
biomass particle diameters	300 μm to 1 mm

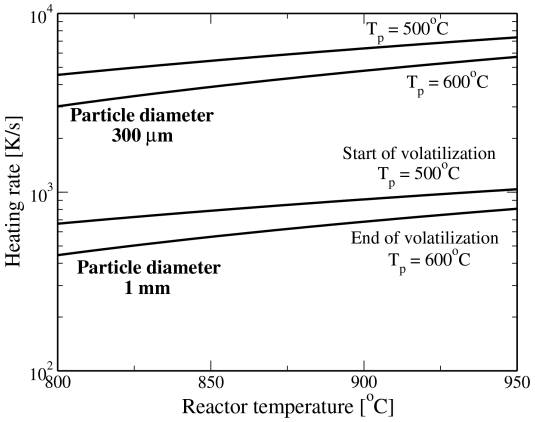

Figure 3. Typical heating rates experienced by the biomass during gasification at the conditions described in Table 1.

3.2. Simulation Configuration. The relative importance of chemical reaction pathways as estimated by the DRGEP reduction methodology depends on the chemical compositions and sample kinetic trajectories on which it is applied. As the reference model is too complex to be used in a realistic reactor configuration, we choose a statistical treatment to sample as broadly as possible the chemical states and trajectories occurring in a gasification reactor. For this purpose, the computationally inexpensive and idealized partially stirred reactor (PaSR) is used. Inside a PaSR, the composition and properties of the fluid are represented by an ensemble of notional particles, each carrying its own species composition and temperature. The properties of each notional particle evolve due to mixing, reaction, and inflow/outflow events such that the mean thermochemical properties of the represented fluid are statistically spatially homogeneous, but the fluid itself is imperfectly mixed at the molecular level. The use of a PaSR as sampling tool forces the reduction to be quite conservative, thereby preventing important pathways to be removed from the reduced kinetic model. It must also be noted that, because a PaSR is not a mathematical representation of a physical system, simulation results cannot not be directly compared to, or interpreted in light of, experimental data.

The fluid is assumed to be an ideal gas-phase mixture that evolves in the PaSR at a constant pressure, so that the full thermochemical state or composition of the mixture Φ is completely characterized by the species mass fractions $\mathbf{Y}$ and the mixture enthalpy $\mathcal{H}$: $\Phi \equiv \{\mathbf{Y}, \mathcal{H}\}$. The PaSR is continuously fed by a user-specified number n_{str} of inflow streams of prescribed compositions Φ_{str}; it will be described later for the biomass system under consideration. At any time t, the reactor contains a constant, even number n_p of notional particles, the i^{th} particle having composition $\Phi^{(i)}(t)$. These compositions evolve in time due to mixing, reaction, and inflow and outflow events. These processes are described in more detail.

Inflow and outflow events occur at discrete times and change the particle composition Φ in a discontinuous manner. In the inflow/outflow event, n_{in} particles are selected at random with equal probability, and their compositions are replaced by the inflow streams' compositions. The integer number n_{in} ($= np \times \Delta t/\tau_{res}$) is chosen according to the specified mean residence time τ_{res} and time step Δt. Between these discrete times, the composition evolves by a mixing fractional step and a reaction fractional step. In the mixing fractional step, particles are paired and ordered so that particles i and i+1 are partners for odd i ($1 \le i < n_p$), and the ordinary differential equations

$$\frac{d\Phi^{(i),m}}{dt} = -\frac{(\Phi^{(i)}(t) - \Phi^{(i+1)}(t))}{\tau_{mix}}$$
$$\frac{d\Phi^{(i+1),m}}{dt} = -\frac{(\Phi^{(i+1)}(t) - \Phi^{(i)}(t))}{\tau_{mix}} \quad (1)$$

DOI: 10.1021/acs.energyfuels.7b01634
Energy Fuels 2017, 31, 12120−12132

are solved for each pair of particles over time interval Δt. In this equation, τ_{mix} is the specified pairwise mixing time scale. At each time step, n_{pair} particles are selected randomly with equal probability and shuffled to change partners. The integer number n_{pair} ($= n_p \times \Delta t/\tau_{pair}$) is chosen according to the specified pairing time τ_{pair}, typically taken equal to τ_{mix}. The compositions after mixing evolve under isobaric, adiabatic conditions over a time Δt according to

$$\frac{d\Phi^{(i),m}(t)}{dt} = \mathbf{S}(\Phi^{(i),m}(t)) \tag{2}$$

where $\mathbf{S}$ is the chemical source term defined by the user-provided reaction mechanism. This reaction fractional step finally yields the particle compositions at $t + \Delta t$: $\Phi^{(i)}(t + \Delta t)$.

The PaSR simulation setup described here will be used to provide relevant compositions of biomass devolatilization products expected to be found in real gasification reactors and to compare the reduced model developed in this section with the reference model.

3.3. Reduction Using DRGEP. The automatic chemical mechanism reduction technique DRGEP[23] is used to extract a reduced model from the reference, detailed model. The reduction procedure follows the steps outlined in Pepiot et al.[23] for species and reaction elimination and is performed using the YARC reduction tool,[35] a Perl/C implementation of DRGEP and associated reduction techniques.

- **Reduction Targets Selection.** The first step in the reduced model development is to identify a set of targets $\mathcal{T}$, most often specific species, that the reduced model must reproduce accurately. In biomass gasification, it is desirable to predict the yield of gaseous products and tar species. Therefore, 5 major gas products: CO, CO_2, H_2, CH_4, and C_2H_4, water (H_2O), and 3 major tar species: benzene (C_6H_6, a single-ring aromatic), naphthalene ($C_{10}H_8$, a polycyclic aromatic), and phenol (C_6H_6O, an oxygenated aromatic) are selected as targets. Moreover, 13 primary devolatilization products described by the reference devolatilization model, such as HAA, HMFU, and LVG, are also incorporated into the targets list.
- **Sample Composition Database.** To evaluate the relative importance of species and reactions for the given set of targets, DRGEP requires an ensemble of sample compositions representative of the simulations in which the reduced model will eventually be used. For this purpose, we use a PaSR configuration and assume that the particles in the PaSR simulation will follow trajectories in composition space that are representative of those they would encounter in an actual reactor. The simulation parameters are chosen based on previous experience and best practices[36] to ensure a broad range of compositions relevant for our application, and the residence time is adjusted to match the characteristic time scale of the overall pyrolysis chemistry process.

  Two inflow streams are continuously fed to the PaSR to represent the release of the primary products from the devolatilizing biomass into the hot nitrogen environment. The first inflow stream consists of nitrogen gas at temperatures varying between 1073 and 1273 K, while the second inflow stream consists of the primary products released during biomass devolatilization. The second stream needs to account for the fact that a gasification reactor contains biomass particles at different stages of devolatilization, acting as variable sources of primary products. To include this variability, the biomass devolatilization process is represented stochastically by sampling from the probability distribution function (PDF) of the extent of biomass devolatilization. This PDF is constructed by simulating biomass devolatilization *a priori* using the reference chemical model.

  The parameters used for these simulations are summarized in Table 2. The PaSR simulations are performed for three nitrogen temperatures: 1073, 1173, and 1273 K. A database of 18,000 distinct chemical compositions is created by randomly sampling the compositions encountered in the PaSR simulations.

Table 2. PaSR Simulation Parameters

parameter	value
number of notional gas particles in PaSR	96
gas residence time	3 s
mixing time	0.3 s
biomass particle heating rates	1000 K/s
temperature of raw biomass	300 K
temperature of pure nitrogen stream	1073−1273 K
normalized mass flow rates of nitrogen stream	0.9
normalized mass flow rates of biomass stream	0.1

- **Automatic Reduction and Error Estimation.** The automatic reduction procedure proceeds through two distinct steps. In the first step, DRGEP analyzes the composition database and quantifies the coupling between species and reactions in the chemical mechanism for the chosen target species in the form of importance coefficients also known as DRGEP coefficients. Species and reactions with the lowest value of DRGEP coefficients are removed from the mechanism in an iterative manner, providing a list of kinetic models of decreasing complexity. More details about the implementation of the DRGEP technique can be found for example in ref 37.

  In the second step, the PaSR test configuration (parameters provided in Table 2) is simulated using each of the reduced models generated in the first stage, and *a posteriori* errors on the targets are computed, defined for any target $\mathcal{T}$ as

$$\varepsilon_{\mathcal{T}} = \frac{\int_0^{t_{end}} |\langle \mathcal{T} \rangle^D(t) - \langle \mathcal{T} \rangle^R(t)| dt}{\int_0^{t_{end}} |\langle \mathcal{T} \rangle^D(t)| dt} \tag{3}$$

In this equation, $\langle \mathcal{T} \rangle(t)$ designates the average of quantity $\mathcal{T}$ at time t over all particles contained in the PaSR, and t_{end} is taken here as 15 PaSR residence times. *A posteriori* errors as a function of the number of species n_S for a few targets are shown in Figure 4. The reduction process provides several mechanisms with decreasing number of species and reactions; we choose the smallest possible mechanism for which the error is less than 10% for most of the species, and at most a factor of 2 for a few groups of species. The mechanism with 60 chemical species and 486 reactions is found to be the smallest acceptable model generated automatically by the DRGEP procedure and is shown by a dotted line in Figure 4.

DOI: 10.1021/acs.energyfuels.7b01634
Energy Fuels 2017, 31, 12120−12132

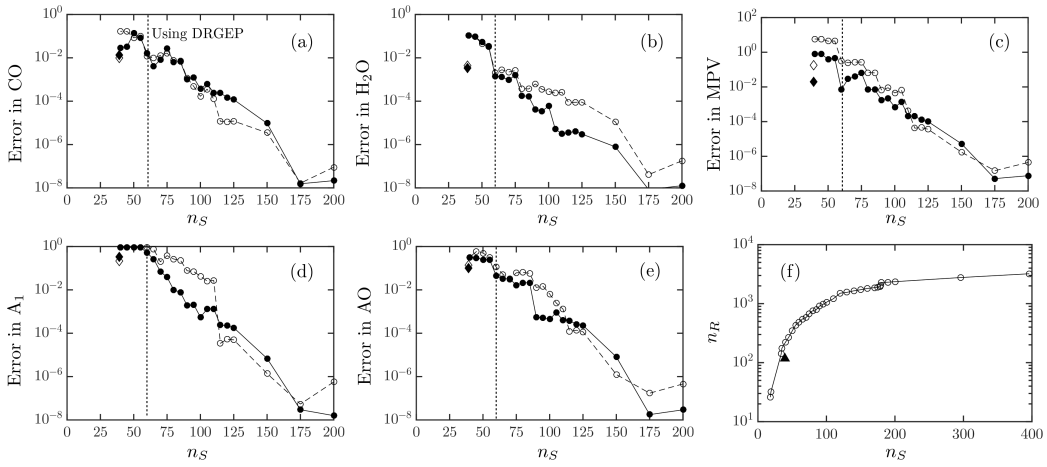

Figure 4. Error in the PaSR predictions as a function of the number of species n_S retained in the skeletal model during the reduction process: (a) CO, (b) H_2O, (c) MPV, (d) A_1, (e) AO, and (f) number of reactions n_R retained in the model. Filled symbols: PaSR nitrogen stream temperature is 1073 K; open symbols: PaSR nitrogen stream temperature is 1273 K. Circles: automatic reduction; diamonds: semiautomatic reduction with quasi-steady-state assumption.

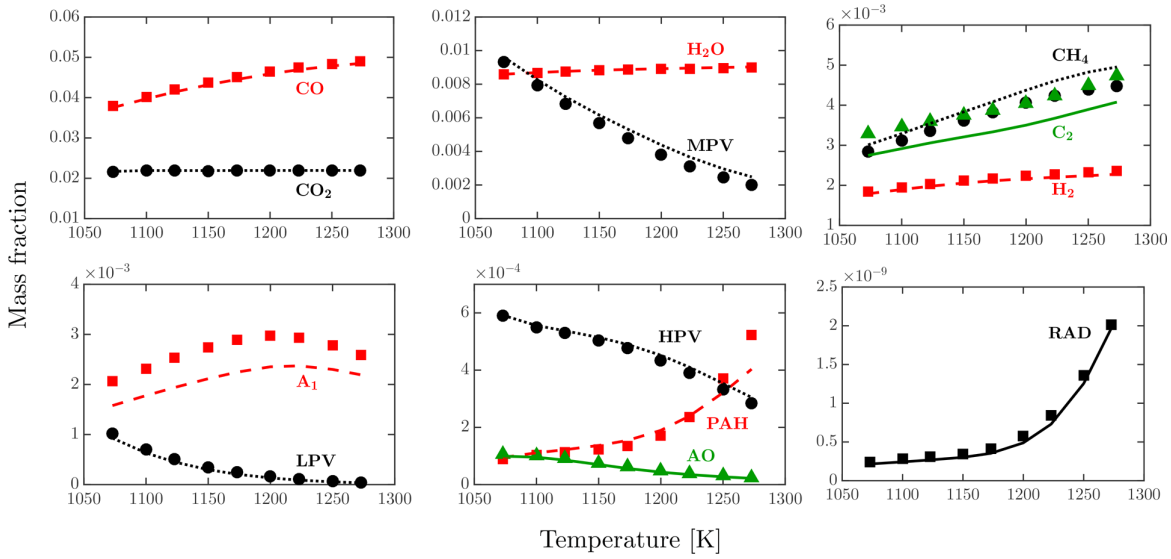

Figure 5. Statistically steady-state mass fractions of various light gases, tar species, devolatilization products, and small radical pool: Comparison between the reduced model (symbols) and the reference chemical model (lines) in a Partially Stirred Reactor (PaSR) configuration for the temperature ranging from 1073 to 1273 K. Expanded species names are provided in Section 4.1.

3.4. Additional Reduction. In the DRGEP technique, a species or a reaction is removed from the chemical mechanism only when it is identified as unimportant for every single composition in the database, which imposes a stringent criterion on species and reaction removal. A species or a reaction can be important for the local dynamics of a target, but may not impact its global statistical behavior. Several techniques have been developed in recent years to identify those additional species and reactions, for example, the DRGEP with the Sensitivity Analysis method.[38] In this work, we use an *ad hoc* semiautomatic technique that quantifies the impact of species and reactions on the global statistical behavior of the targets. This technique utilizes the global production/consumption rates of each species for every reaction obtained from the simulations of the PaSR test configuration using the intermediate mechanism. The coupling between species and reactions on the targets is quantified in a manner similar to the DRGEP technique, but using the global production and consumption rates of species instead. Potential species and reactions that may have a minimal impact on the prediction of global statistics of the targets are removed from the mechanism, and the resulting model is simulated in the PaSR test configuration to calculate *a posteriori* errors on the targets using eq 3. A 44 species and 118 reactions mechanism is found to be the smallest acceptable model after this step and is shown by diamond symbols in Figure 4.

3.5. Quasi-Steady-State Approximations. Once the above-mentioned strategies have removed as many species and reactions as possible, quasi-steady-state (QSS) approximations are introduced that replace the differential equation for a given species by an algebraic expression much faster to solve. All suitable QSS species are computed using algebraic

DOI: 10.1021/acs.energyfuels.7b01634
Energy Fuels 2017, 31, 12120−12132

expressions consisting of non-QSS species. To keep the calculation of QSS species simple and fast, it is made sure that all of the algebraic expressions are linear.[39] With this constraint, 5 QSS species are identified: C_2H_5, CH_2OH, CH_2CHO, C_7H_7, and CH_2CO.

The final reduced kinetic model has 39 non-QSS species (including N2), 118 reactions (including both forward and backward reactions), and 5 QSS species.

4. VALIDATION OF THE REDUCED MODEL

In this section, the accuracy of the reduced model (39 species and 118 reactions) developed in Section 3 is assessed for a number of configurations. Three different test cases are performed: (1) The PaSR test configuration is simulated using both the reduced and the reference models, and major product and tar species are compared. (2) The reduced model is used in a zero-dimensional reactor configuration to simulate the pyrolysis experiments of Shin et al.[33] (3) The reduced model is integrated with the CFD solver NGA[40] to simulate biomass gasification in the laboratory-scale Drop Tube Reactor (DTR) of Chen et al.[41] These validation cases are discussed in the following subsections. Additional validation considering the pyrolysis of phenol can be found in the Supporting Information document.

4.1. Comparison in a Partially Stirred Reactor. The PaSR configuration used to create the composition database in Section 3 is used again here to compare the reduced model to the reference model for the temperatures ranging from 1073 to 1273 K. The parameters used for these simulations are shown in Table 2. After a statistically steady state is reached, the mass fractions of gaseous products and tar species are averaged over 10 residence times to get mean steady-state mass fractions. Since the reaction pathways are significantly altered due to the high reduction ratio, the mass fraction of a few species are not compared individually. Instead, these species are divided into different groups based on their molecular weights, and the sum of their mass fractions is compared.

Figure 5 compares the mean steady-state mass fractions of relevant individual species and groups of species obtained from the reduced and reference models. Predictions of the reduced and reference models for major product gases: CO, CO_2, CH_4, H_2, and C_2 (species with 2 carbon atoms), water (H_2O), and three classes of tars: single-ring aromatics (A_1), polycyclic aromatic hydrocarbons (PAH), and oxygenated aromatics (AO) are in good agreement. In addition, the reduced model is also able to predict light (LPV), medium (MPV), and heavy (HPV) weight primary devolatilization products, and small radicals pool (RAD). Those acronyms and their definitions are summarized in Table. 3. Note that the assumption of constant heating rate used in the reduction procedure is shown to have negligible impact on the results, as is described in the Supporting Information document.

The PaSR simulations are carried out on a Beowulf cluster with Nehalem X series processors. The time per iteration per processor for using the reduced model is $O(10^{-3}$ s) and for the reference model it is $O(10^{-1}$ s), corresponding to a reduction in the CPU time by ~99% by the reduced model. It must be noted that in the PaSR simulations the majority of the time is spent on the integration of the chemical source terms; therefore, the saving in the CPU time is dominated by this term. Reduction in computational expense is expected to be even higher in CFD simulations as additional scalar transport equations need to be solved for each species at every grid point in the computational domain.

Table 3. List of Species and Group of Species, and Their Acronyms

acronyms	name
A_1	single ring aromatics (e.g., benzene)
AO	oxygenated aromatics (e.g., phenol)
C_2	gases containing two carbon atoms (e.g., ethylene)
HAA	hydroxyacetaldehyde
HMF	hydroxymethyl furfural
HPV	heavy weight primary vapors (7+ carbon atoms, e.g., *p*-coumaryl)
MPV	medium weight primary vapors (4−6 carbon atoms, e.g., levoglucosan)
LPV	light weight primary vapors (2−3 carbon atoms, e.g., glyoxal)
LVG	levoglucosan
PAH	polycyclic aromatic hydrocarbons (e.g., naphthalene)
RAD	small radicals pool (e.g., H, OH)

4.2. Pyrolysis in a Tubular Reactor. The reduced model is used to simulate the tubular reactor experiments of Shin et al.[33] described in Section 2.2. Simulation results are compared with the experimental measurements in Figure 6 and show overall a good agreement. When compared to the simulations performed with the detailed, reference mechanism (Figure 1), we see that the prediction of hydroxymethyl furfural decomposition is virtually unchanged by the reduction process, but more significant changes are observed for levoglucosan and hydroxyacetaldehyde, for which the decomposition rate has been reduced. While agreement with the experimental data is still satisfactory, those results indicate a larger sensitivity of those molecules to the underlying small radical chemistry.

4.3. Fast Pyrolysis of Biomass in a Drop Tube Reactor. Numerical simulations of the one-dimensional DTR of Chen et al.[41] are conducted and compared to the experimental results. A schematic of the experimental DTR can be seen in Figure 7. Chen et al.[41] studied fast pyrolysis of millimetric sized biomass particles (beech wood) in the DTR at 1073 and 1223 K. In the experiments, particles are flake-like and are characterized by their equivalent spherical diameters. Biomass particles and nitrogen stream are continuously injected from the top of the reactor, while the exhaust gas is sampled at the bottom. A portion of this exhaust gas is then examined by several gas analyzers. The distance between the locations of biomass injection and gas collection is varied to get four residence lengths: 0.3, 0.5, 0.7, and 0.9 m. The total amount of gas, tar, and char produced is measured at these residence lengths. Moreover, yields of major gas-phase components are also provided.

The DTR presents a multiphase and multiphysics system; therefore, simulations of this reactor require a reactive multiphase flow solver. For this purpose, the reduced model and the biomass devolatilization model are integrated with the reactive multiphase CFD solver NGA,[40] with a Euler−Lagrange strategy[42] to model gas−solid flows. NGA has been extensively validated and used for various DNS and LES multiphase reactive flow systems.[43−50] Simulations were conducted for biomass particles with the equivalent spherical diameter (d_p) of 520 μm and two gas temperatures: T = 1073 K (simulation $\mathcal{S}1$) and 1223 K (simulation $\mathcal{S}2$). Parameters used for $\mathcal{S}1$ and $\mathcal{S}2$ are provided in Table 4. In the DTR simulations, two modeling issues are encountered related to (1) the reference devolatilization kinetics model and (2) the shape of the particles. These are

DOI: 10.1021/acs.energyfuels.7b01634
Energy Fuels 2017, 31, 12120−12132

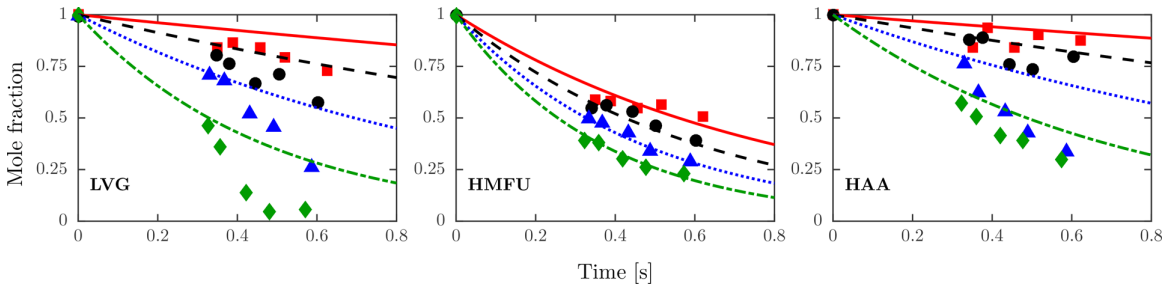

Figure 6. Pyrolytic decomposition of levoglucosan (LVG), hydroxyacetaldehyde (HAA), and hydroxymethyl furfural (HMFU): Comparison between simulation results using the reduced kinetic model (lines) and experiments (symbols, Shin et al.[33]). Different symbols indicate different temperatures (square: 898 K, circle: 923 K, triangle: 948 K, and diamond: 973 K).

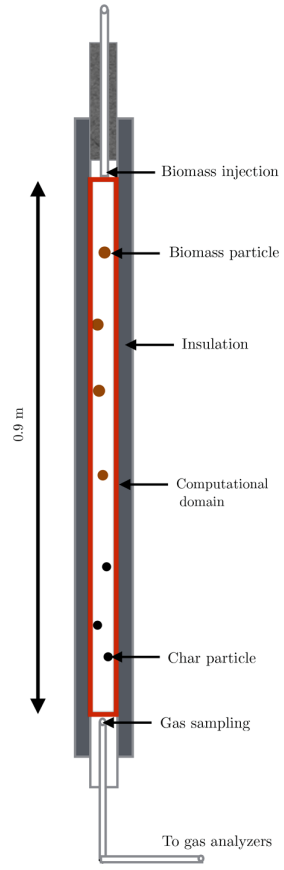

Figure 7. Schematic of the experimental Drop Tube Reactor;[41] the computational domain considered in this study is indicated in red.

discussed in the following two subsections before the results of the DTR simulations are presented.

Biomass Devolatilization Model. In the DTR simulations, the biomass devolatilization chemistry is modeled by the reference devolatilization model discussed in Section 2.1. Preliminary DTR simulations could not accurately predict the experimental yields of CH_4, C_2H_4, and solid residue. This difference is attributed to the fact that a significant portion of these two gases remains trapped in the solid matrix in the chemisorbed state. For simulation $\mathcal{S}1$, Figure 8a shows the evolution of the trapped species ($\mathcal{T}_{sp} \equiv$ CO, CO_2, and CH_3OH) that are completely released from the biomass particle during the devolatilization, whereas Figure 8b shows

Table 4. Parameters for the Drop Tube Reactor Simulation

parameter	value
domain length ($L_x \times L_y \times L_z$)	0.9 m × 0.02 m × 0.02 m
number of cells ($n_x \times n_y \times n_z$)	900 × 1 × 1
inlet nitrogen velocity	0.279 m/s
temperature of inlet nitrogen stream	1073 K ($\mathcal{S}1$) and 1223 K ($\mathcal{S}2$)
injection rate of biomass particles	7.545×10^{-7} kg/s
biomass density	710 kg/m^3
biomass particle size	520 μm
biomass composition (wt %)	
cellulose	43.91
hemicellulose	23.85
C-rich lignin	3.24
H-rich lignin	14.99
O-rich lignin	6.71
ash	0.4
moisture	6.9

that a few trapped species ($\mathcal{T}^*_{sp} \equiv COH_2$, CH_4, C_2H_4, and H_2) remain inside the biomass particle even after the complete devolatilization. Figure 8c shows that, even long after the completion of biomass devolatilization, the amount of solid residue is much higher than that of char; this difference is also attributed to the trapped species $\mathcal{T}^*_{sp}$. This is corroborated by the fact that the predicted value of char, $Y_{char} = 0.10$, is close to the solid residue measured in the experiments, $SR_{exp} = 0.08 \pm 20\%$.

Similar discrepancies have been very recently investigated by Anca-Couce et al.,[51] who performed biomass pyrolysis experiments and used the reference devolatilization model to predict the experimental yields of various species. They introduced several modifications in the devolatilization mechanism to significantly improve the agreement between the modeled results and their experimental database, mainly for the yields of light hydrocarbons and the yield and composition of char. The focus of the present paper being the secondary gas-phase reactions, we introduce here a simple *ad hoc* modification of the Corbetta et al. model[24] considering only the current experiment at hand, as described below, and refer the reader to the study of Anca-Couce et al.[51] for a more comprehensive treatment of this issue. To improve the predictions of CH_4, C_2H_4, and solid residue, we adjust the parameters of the reactions, present in the reference devolatilization model, governing the release of $\mathcal{T}^*_{sp}$. In the reference devolatilization model, activation energies (E_{act}) for the release of $\mathcal{T}^*_{sp}$ are much

DOI: 10.1021/acs.energyfuels.7b01634
Energy Fuels 2017, 31, 12120−12132

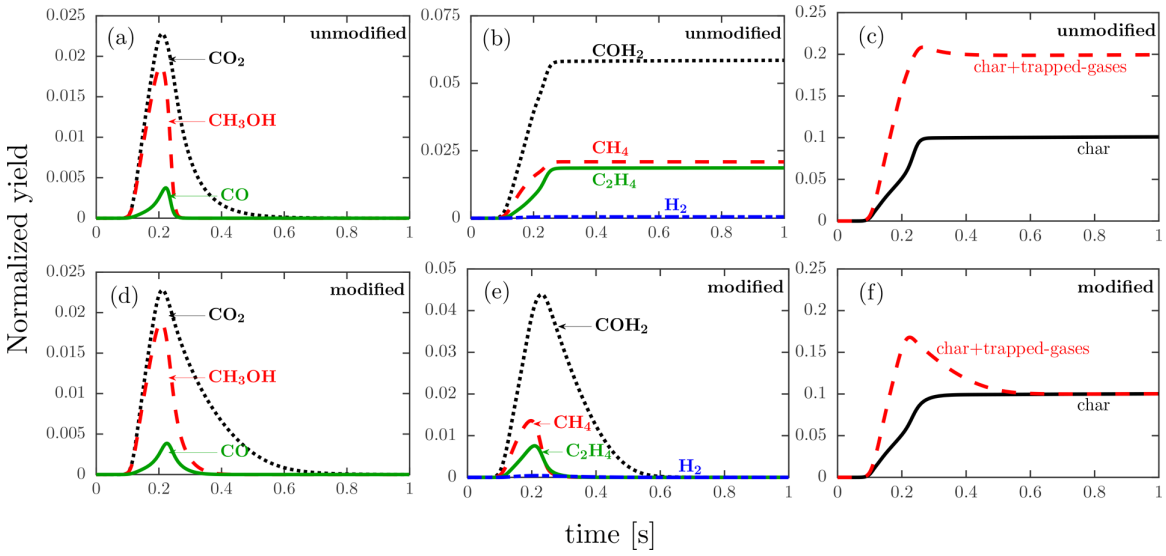

Figure 8. Evolution of trapped species, char, and solid residue during biomass devolatilization in DTR simulation $\mathcal{S}1$ using the unmodified reference devolatilization model described in Section 2.1 (first row) and the modified model described in section 4.3 (second row). (a) and (d) show the evolution of trapped species that are completely released from the biomass using the unmodified and modified devolatilization model, respectively. (b) and (c) show that for the original devolatilization model some trapped species are not released from the biomass, while those trapped species are released after the modification as shown in (e) and (f). Yields are normalized with the initial mass of biomass particle.

higher compared to E_{act} for the release of $\mathcal{T}_{sp}$. To make the release of $\mathcal{T}^*_{sp}$ faster, we replace the E_{act} for the release of $\mathcal{T}^*_{sp}$ by the E_{act} for the release of trapped CO. Simulation $\mathcal{S}1$ is repeated with the modified values of the E_{act}; the resulting evolution profiles of $\mathcal{T}_{sp}$ and $\mathcal{T}^*_{sp}$ are shown in Figures 8d and 8e, respectively, and the evolution of char and solid residue is shown in Figure 8f. These figures show that, as the devolatilization proceeds, all the trapped species get released from the biomass particles and the amount of solid residue, $SR_{sim} = 0.1$, is close to the experimental value, $SR_{exp} = 0.08 \pm 20\%$. Therefore, the reference devolatilization model with the modified value of E_{act} for $\mathcal{T}^*_{sp}$ is used in the DTR simulations.

Shape of the Particles. Biomass particles used in the experiments have a flake-like shape. The shape of the particle affects the drag force from the surrounding gas and the heat transfer rate experienced by the particle. In the simulations, particles are treated as spheres; therefore, a correction must be made to include the effect of the proper particle shape while calculating drag force and heat transfer rate. Chen[52] experimentally measured the slip velocity of the biomass particles and estimates a correction factor of **1.5** that can be multiplied with the drag correlation for a spherical particle to estimate the drag on a flake-like particle. In the DTR simulations, this correction factor is used in the drag calculation for the biomass particles. Although drag is corrected for the flake-shaped particles, any correction for heat transfer rate is not provided in the experimental study. Therefore, we calculate correction factors to estimate the convective and radiative heat transfer rates of the flake-shaped particles based on the calculation for spherical particles.

Convective heat transfer rate for a particle can be expressed as

$$q_{conv} = hA\Delta T \tag{4}$$

where A is the surface area of the particle, Δt is the temperature difference between the particle surface and the surrounding gas, and h is the convective heat transfer coefficient. h can be calculated from the Nusselt number, Nu, as $h = \frac{Nu\lambda_f}{l}$, where λ_f is thermal conductivity of the gas surrounding the particle and l is the characteristic length, which is equal to the diameter (d_p) for a sphere and the thickness (t_p) for a flake-shaped particle. The Nusselt number is calculated using Gunn's correlation.[34] Average area of the flake-shaped particles is calculated based on the experimental measurements[52] of particle dimensions. The ratio of the average area of the flake-shaped particles (A^*) to that of an equivalent spherical particle (A) is calculated to be **1.33**. Using the thickness, t_p, as the characteristic length in the expression for h, the convective heat transfer rate for the flake-shaped particles becomes

$$q^*_{conv} = \left(\frac{d_p}{t_p}h\right)\left(\frac{A^*}{A}A\right)\Delta T \tag{5}$$

For a biomass particle of equivalent diameter $d_p = 520\ \mu$m, the experimentally measured average particle thickness (t_p) is 250 μm. Substituting these values in eq 5, we get

$$q^*_{conv} = \left(\frac{520}{250}h\right)(1.33A)\Delta T \sim 2.8hA\Delta T = 2.8q_{conv} \tag{6}$$

Equation 6 implies that the convective heat transfer rate for the flake-shaped particles (corresponding to an equivalent spherical diameter of 520 μm) is about 2.8 times faster than that for the equivalent spherical particles.

The radiative heat transfer rate from the reactor walls to the biomass particle is modeled by

$$q_{rad} = A\omega_p\sigma(T^4_{wall} - T^4_p) \tag{7}$$

where ω_p is the particles emissivity, σ is the Stefan–Boltzmann constant ($= 5.6704 \times 10^{-8}\ \mathrm{Wm^{-2}\ K^{-4}}$), T_{wall} is the reactor wall

DOI: 10.1021/acs.energyfuels.7b01634
Energy Fuels 2017, 31, 12120−12132

temperature, and T_p is the particle surface temperature. ω_p is calculated as a linear combination of wood ($\omega_w = 0.7$) and char emissivity ($\omega_c = 0.92$).[53] For a flake-shaped particle, A is replaced by A^*, and we get

$$q^*_{rad} = \left(\frac{A^*}{A}\right) A\omega_p\sigma(T^4_{wall} - T^4_p) = 1.33q_{rad} \quad (8)$$

Equation 8 implies that the radiative heat transfer rate for the flake-shaped particles (corresponding to an equivalent spherical diameter of 520 μm) will be about 1.33 times faster than that of the equivalent spherical particles.

To evaluate the effect of these corrections for convective and radiative heat transfer rates on biomass devolatilization, $\mathcal{S}1$ is performed with the corrected rates (q^*_{conv} and q^*_{rad}) and the uncorrected rates (q_{conv} and q_{rad}). Figure 9 shows that using the corrected heat transfer rates significantly improves the prediction of the shrinkage rate of the particles. Therefore, in the DTR simulations, convective and radiative heat transfer rates for the spherical particles are multiplied with 2.8 and 1.33, respectively, to make correction for the shape of the particles.

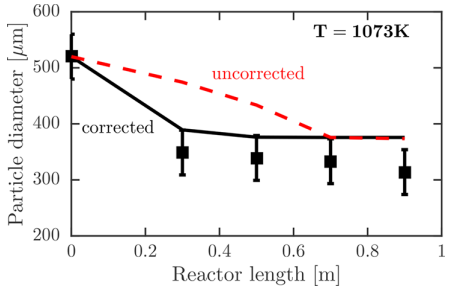

Figure 9. Biomass diameter (for simulation $\mathcal{S}1$) at various reactor lengths: Comparison between experimental measurements (symbols), and simulation predictions with corrected heat transfer rate (solid line) and uncorrected heat transfer rate (dashed line).

Comparison with Experimental Data. After incorporating the modifications in the reference devolatilization model and the heat transfer rates, simulations $\mathcal{S}1$ and $\mathcal{S}2$ are run until steady state is reached. Figure 10 compares the simulation predictions of the mass fraction of major gas products and particle diameters at various reactor lengths to the experimental values. Agreement between the simulation predictions and experimental measurements is very good considering the possibility of the high degree of variability in various parameters and physical properties. These simulations are performed on a single core of a MacBook laptop and required O(1 hour) to reach steady state, which shows the affordability of the current reduced model to simulate laboratory-scale reactors.

5. APPLICATION TO A FLUIDIZED BED REACTOR

The reduced gas-phase chemistry model, coupled with the biomass devolatilization model of Corbetta et al.,[24] is used to simulate a pseudo-2D configuration (rectangular geometry) of an experimental FBR[54] using NGA.[40] Parameters used in this simulation are reported in Table 5. Initially, the sand bed is fluidized without biomass particles by injecting the nitrogen gas from the bottom of the reactor. Once a fluidized sand bed is

Table 5. Parameters for the FBR Simulation

parameter	value
domain length ($L_x \times L_y \times L_z$)	0.15 m × 0.02 m × 0.0015 m
number of cells ($n_x \times n_y \times n_z$)	300 × 40 × 3
inlet nitrogen velocity	0.2 m/s ($6u_{mf}$)
inlet nitrogen temperature	1073 K
number of sand particles	10^5
size of sand particles	200 μm
density of sand particles	2650 kg/m^3
injection rate of biomass particles	5×10^{-6} kg/s
size of biomass particles	200 μm
density of biomass particles	907 kg/m^3
biomass composition (wt %)	
CELL	47.24
HCELL	31.49
LIGC	2.78
LIGH	6.48
LIGO	4.63
ash	0.37
moisture	7.0

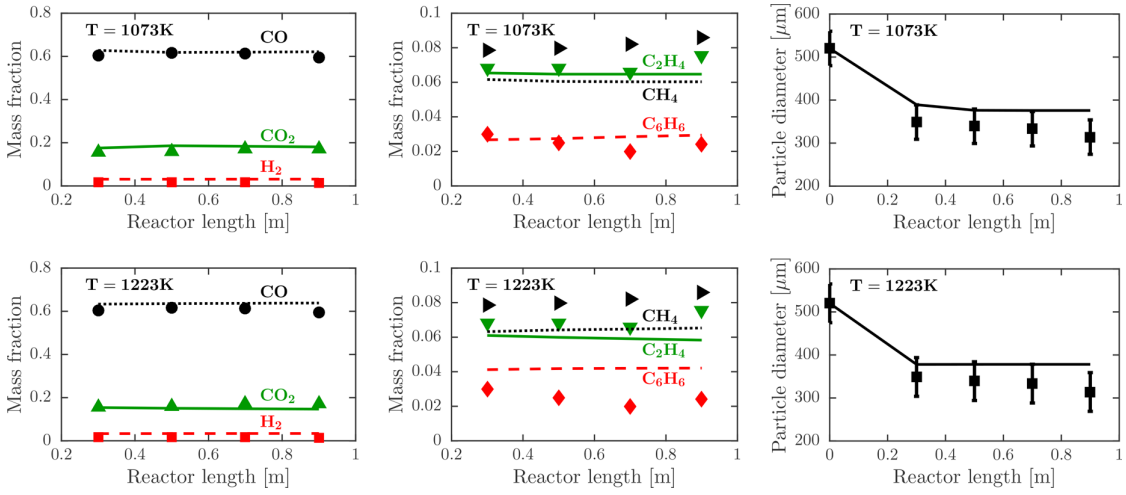

Figure 10. Steady-state mass fraction (dry basis) of various gas species and particle diameter at different reactor lengths: Comparison between simulation results (lines) and experimental measurements (symbols) for particle diameter, d_p = 520 μm, and two gas temperatures: 1073 and 1223 K.

DOI: 10.1021/acs.energyfuels.7b01634
Energy Fuels 2017, 31, 12120−12132

achieved, biomass particles are injected into the reactor at a constant mass flow rate. Simulation is run long enough to reach a statistically steady state. Figure 11 shows the instantaneous

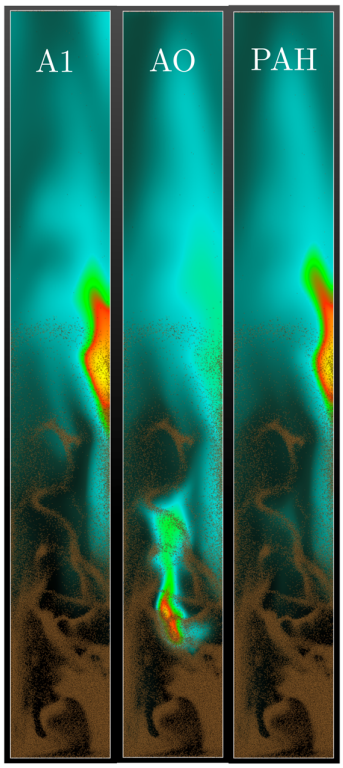

Figure 11. Instantaneous mass fraction of different classes of tar: A_1 (single-ring aromatics), AO (oxygenated aromatics), and PAH (poly aromatic hydrocarbons), scaled by their individual maxima in the pseudo two-dimensional FBR simulation.

values of the mass fraction of various classes of tar normalized by their maxima at statistically steady state. The location of the mass fraction maximum of oxygenated aromatics (AO) is very different from that of single-ring (A_1) and multiple-ring (PAH) aromatics. It indicates that different tar species can have different length and time scales associated with their formation and consumption. The mass fractions of the major gas and tar species at different reactor lengths are shown in Figure 12. As expected, CO is the major gas product, followed by CO_2, CH_4, C_2, and H_2. Among tars, single-ring aromatics are the major species, followed by oxygenated aromatics, and polycyclic aromatic hydrocarbons (PAH). Another important observation made from Figure 12 is that the mass fraction of all the light gases, and A_1 and PAH increase along the reactor height, while it decreases for AO.

The simulation was performed on 96 cores on the cluster mentioned in Section 4.1 and required 3000 CPU hours and 9000 CPU hours per flow-through time (0.75 s) for the pure sand fluidization case and the reacting case with biomass injection, respectively. This simulation shows the ability of the reduced model to be used with a CFD solver to simulate laboratory-scale FBR in an affordable manner. The present reduced model combined with a CFD solver provides the capability to track the evolution of major gas and tar species for different operating conditions.

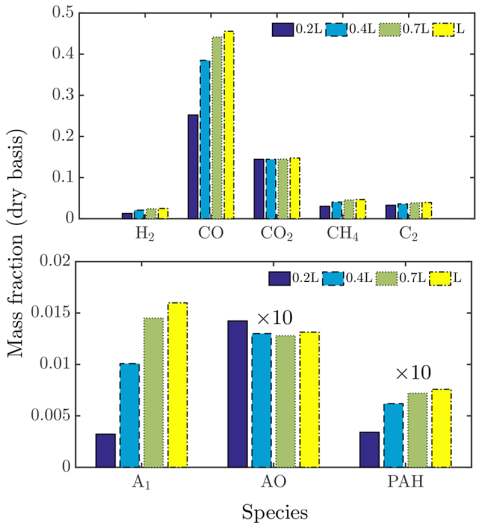

Figure 12. Steady-state mass fraction of major gas and tar species at different reactor lengths in the pseudo two-dimensional FBR simulation. Mass fractions of AO and PAH are multiplied by 10 to compare their behavior with A_1.

6. CONCLUSION

An adequate description of the chemical kinetics in the CFD tools is imperative for the detailed simulations of biomass gasification; however, the large size of detailed mechanisms makes their use prohibitive in the CFD simulations. In this work, we assemble a detailed chemical model (396 species, 3210 reactions) for the secondary gas-phase reactions of biomass gasification and reduce it to a compact model (39 species, 5 quasi-steady-state species, and a total of 118 reactions) using automated strategies. The reduced model shows very good reproducibility of the statistical yields of various species of interest at a fraction of computational cost compared to the detailed model. The savings in computational time are expected to be higher in CFD simulations where a set of extra partially differential equations (PDEs) need to be solved for the scalar transport equations. The reduced model, integrated with the CFD solver NGA, is used to simulate a laboratory-scale drop tube reactor (DTR) experiment showing good agreement with the experiments. By simulating a pseudo two-dimensional FBR with the reduced model, it is shown that an adequate description of the gas-phase reactions can be used with CFD tools in a computationally affordable manner. The reduced model developed here is small enough to be integrated with a CFD solver to study the secondary gas-phase reactions of biomass gasification in laboratory-scale reactors.

■ ASSOCIATED CONTENT

Supporting Information

The Supporting Information is available free of charge on the ACS Publications website at DOI: 10.1021/acs.energyfuels.7b01634.

Additional validation cases for the reference kinetic model and the reduced model; Partially Stirred Reactor case with a variable heating rate; and the reduced kinetic model in CHEMKIN format along with the thermodynamic and transport data for all the gas-phase species (PDF)

DOI: 10.1021/acs.energyfuels.7b01634
Energy Fuels 2017, 31, 12120−12132

AUTHOR INFORMATION

Corresponding Author

*E-mail: pp427@cornell.edu.

ORCID

Himanshu Goyal: 0000-0001-5387-632X

Notes

The authors declare no competing financial interest.

ACKNOWLEDGMENTS

This material is based in part upon work supported by the National Science Foundation under Grant Number EEC-1342362.

NOMENCLATURE

A=surface area of biomass particle based on an equivalent diameter (Section 4.3, m^2)
A^*=surface area of biomass particle derived from experimental data (Section 4.3, m^2)
d_p=equivalent diameter of biomass particle (Section 4.3, m)
E_{act}=activation energy (J/mol)
$\mathcal{H}$=enthalpy (J)
h=convective heat transfer coefficient (W/m^2K)
l=characteristic length of biomass particle (m)
n_{in}=number of inflowing particles per time step in the PaSR
n_p=number of particles in the PaSR
n_{pair}=number of particles changing partners per time step in the PaSR
n_R=number of reactions in kinetic model
n_S=number of species in kinetic model
n_{str}=number of inflowing streams in the PaSR
Nu=Nusselt number
q_{conv}=convective heat transfer rate (J/s)
q^*_{conv}=corrected convective heat transfer rate (J/s)
q_{rad}=radiative heat transfer rate (J/s)
q^*_{rad}=corrected radiative heat transfer rate (J/s)
$\mathbf{S}$=chemical source term in the PaSR
SR_{exp}=solid residue in experiment (Section 4.3)
SR_{sim}=solid residue in simulation (Section 4.3)
$\mathcal{S}1$, $\mathcal{S}2$=simulation cases (Section 4.3)
T=gas-phase temperature (K)
T_p=biomass particle temperature (K)
T_{wall}=wall temperature (Section 4.3, K)
t=time (s)
t_{end}=integration time to calculate the errors for the targets (s)
t_p=thickness of biomass particles (Section 4.3, m)
$\mathcal{T}$=set of targets used in DRGEP
$\langle\mathcal{T}\rangle^D$=average value of target $\mathcal{T}$ in the PaSR using the detailed model
$\langle\mathcal{T}\rangle^R$=average value of target $\mathcal{T}$ in the PaSR using the reduced model
$\mathcal{T}_{sp}$=trapped species that are released from biomass during devolatilization
$\mathcal{T}^*_{sp}$=trapped species that remain inside biomass after devolatilization
$\mathbf{Y}$=species mass fractions
Y_{char}=char yield (Section 4.3)
ΔT=temperature difference between biomass particle surface and the surrounding gas (K)
Δt=PaSR simulation time step (s)
$\epsilon_{\mathcal{T}}$=*a posteriori* error on target $\mathcal{T}$
Φ=composition of the mixture in the PaSR
Φ^i=composition of the i^{th} particle in the PaSR
Φ^m=composition of the mixture after the mixing fractional step in the PaSR
Φ_{str}=composition of the PaSR inflow stream
λ_f=gas thermal conductivity (W/m.K)
τ_{mix}=particle mixing time scale in the PaSR (s)
τ_{pair}=particle pairing time scale in the PaSR (s)
τ_{res}=residence time in the PaSR (s)
σ=Stefan–Boltzmann constant
ω_c=char emissivity
ω_p=biomass particle emissivity
ω_w=wood emissivity

REFERENCES

(1) Palma, C. F. *Appl. Energy* **2013**, *111*, 129–141.
(2) Van Paasen, S.; Kiel, J.; Veringa, H. *Tar formation in a fluidised bed gasifier*; Report ECN-04-013; ECN: Petten, The Netherlands, **2004**.
(3) Van der Hoef, M. A.; van Sint Annaland, M.; Deen, N. G.; Kuipers, J. A. M. *Annu. Rev. Fluid Mech.* **2008**, *40*, 47–70.
(4) Gómez-Barea, A.; Leckner, B. *Prog. Energy Combust. Sci.* **2010**, *36*, 444–509.
(5) Debiagi, P. E. A.; Gentile, G.; Pelucchi, M.; Frassoldati, A.; Cuoci, A.; Faravelli, T.; Ranzi, E. *Biomass Bioenergy* **2016**, *93*, 60–71.
(6) Norinaga, K.; Shoji, T.; Kudo, S.; Hayashi, J.-i. *Fuel* **2013**, *103*, 141–150.
(7) Bruchmuller, J.; van Wachem, B.; Gu, S.; Luo, K.; Brown, R. *AIChE J.* **2012**, *58*, 3030–3042.
(8) Bruchmüller, J.; Luo, K. H.; Van Wachem, B. G. M. *Proc. Combust. Inst.* **2013**, *34*, 2373–2381.
(9) Ku, X.; Li, T.; Løvås, T. *Energy Fuels* **2015**, *29*, 5127–5135.
(10) Miller, R.; Bellan, J. *Combust. Sci. Technol.* **1997**, *126*, 97–137.
(11) Fletcher, D.; Haynes, B.; Christo, F.; Joseph, S. *Applied mathematical modelling* **2000**, *24*, 165–182.
(12) Xiong, Q.; Aramideh, S.; Kong, S.-C. *Energy Fuels* **2013**, *27*, 5948–5956.
(13) Xiong, Q.; Kong, S.-C.; Passalacqua, A. *Chem. Eng. Sci.* **2013**, *99*, 305–313.
(14) Xue, Q.; Heindel, T. J.; Fox, R. O. *Chem. Eng. Sci.* **2011**, *66*, 2440–2452.
(15) Xue, Q.; Dalluge, D.; Heindel, T.; Fox, R.; Brown, R. *Fuel* **2012**, *97*, 757–769.
(16) Mellin, P.; Kantarelis, E.; Yang, W. *Fuel* **2014**, *117*, 704–715.
(17) Oevermann, M.; Gerber, S.; Behrendt, F. *Particuology* **2009**, *7*, 307–316.
(18) Oevermann, M.; Gerber, S.; Behrendt, F. Euler–Lagrange modeling of wood gasification in fluidized beds. In *Proceedings of the 9th International Conference on Circulating Fluidized Beds*, 2008; pp 733–738.
(19) Papadikis, K.; Gu, S.; Bridgwater, A. *Chem. Eng. Sci.* **2009**, *64*, 1036–1045.
(20) Papadikis, K.; Gu, S.; Bridgwater, A. V. *Chem. Eng. J.* **2009**, *149*, 417–427.
(21) Ku, X.; Li, T.; Løvås, T. *Chem. Eng. Sci.* **2015**, *122*, 270–283.
(22) Løvås, T.; Houshfar, E.; Bugge, M.; Skreiberg, Ø. *Energy Fuels* **2013**, *27*, 6979–6991.
(23) Pepiot-Desjardins, P.; Pitsch, H. *Combust. Flame* **2008**, *154*, 67–81.
(24) Corbetta, M.; Frassoldati, H. A.; Bennadji; Smith, M. J. K.; Serapiglia; Gauthier, G.; Melkior, T.; Ranzi, E.; Fisher, E. M. *Energy Fuels* **2014**, *28*, 3884–3898.
(25) Ranzi, E.; Cuoci, A.; Faravelli, T.; Frassoldati, A.; Migliavacca, G.; Pierucci, S.; Sommariva, S. *Energy Fuels* **2008**, *22*, 4292–4300.
(26) Calonaci, M.; Grana, R.; Barker Hemings, E.; Bozzano, G.; Dente, M.; Ranzi, E. *Energy Fuels* **2010**, *24*, 5727–5734.

DOI: 10.1021/acs.energyfuels.7b01634
Energy Fuels 2017, 31, 12120–12132

(27) Blanquart, G.; Pepiot-Desjardins, P.; Pitsch, H. *Combust. Flame* **2009**, *156*, 588−607.
(28) Narayanaswamy, K.; Blanquart, G.; Pitsch, H. *Combust. Flame* **2010**, *157*, 1879−1898.
(29) Narayanaswamy, K.; Pepiot, P.; Pitsch, H. Jet fuels and Fischer-Tropsch fuels: Surrogate definition and chemical kinetic modeling. In *U.S. National Combustion Meeting*, Salt Lake City, Utah, May 19−22, 2013.
(30) Narayanaswamy, K.; Pepiot, P.; Pitsch, H. *Combust. Flame* **2014**, *161*, 866−884.
(31) Narayanaswamy, K.; Pitsch, H.; Pepiot, P. *Combust. Flame* **2015**, *162*, 1193−1213.
(32) Narayanaswamy, K.; Pitsch, H.; Pepiot, P. *Combust. Flame* **2016**, *165*, 288−309.
(33) Shin, E.-J.; Nimlos, M. R.; Evans, R. J. *Fuel* **2001**, *80*, 1697−1709.
(34) Gunn, D. *Int. J. Heat Mass Transfer* **1978**, *21*, 467−476.
(35) Pepiot, P. Automatic strategies to model transportation fuel surrogates. Ph.D. Thesis, Department of Mechanical Engineering, Stanford University, Standford, CA, 2008.
(36) Liang, Y.; Pope, S. B.; Pepiot, P. *Combust. Flame* **2015**, *162*, 3236−3253.
(37) Mehta, M.; Fox, R. O.; Pepiot, P. *Ind. Eng. Chem. Res.* **2015**, *54*, 5407−5415.
(38) Niemeyer, K. E.; Sung, C.-J.; Raju, M. P. *Combust. Flame* **2010**, *157*, 1760−1770.
(39) Pepiot-Desjardins, P.; Pitsch, H. *Combust. Theory Modell.* **2008**, *12*, 1089−1108.
(40) Desjardins, O.; Blanquart, G.; Balarac, G.; Pitsch, H. *J. Comput. Phys.* **2008**, *227*, 7125−7159.
(41) Chen, L.; Dupont, C.; Salvador, S.; Grateau, M.; Boissonnet, G.; Schweich, D. *Fuel* **2013**, *106*, 61−66.
(42) Capecelatro, J.; Desjardins, O. *J. Comput. Phys.* **2013**, *238*, 1−31.
(43) Desjardins, O.; Pitsch, H. Modeling Effect of Spray Evaporation on Turbulent Combustion; Paper ID ICLASS06-084. In *10th International Conference on Liquid Atomization and Spray Systems*, Kyoto, Japan, Aug 27−Sept 1, 2006.
(44) Wang, L.; Pitsch, H. Prediction of pollutant emissions from industrial furnaces using large eddy simulation. In *5th U.S. Combustion Meeting*, San Diego, CA, March 25−28, 2007.
(45) Knudsen, E.; Pitsch, H. *Combust. Flame* **2008**, *154*, 740−760.
(46) Desjardins, O.; Moureau, V.; Pitsch, H. *J. Comput. Phys.* **2008**, *227*, 8395−8416.
(47) Desjardins, O.; Pitsch, H. *J. Comput. Phys.* **2009**, *228*, 1658−1677.
(48) Knudsen, E.; Pitsch, H. *Combust. Flame* **2009**, *156*, 678−696.
(49) Pepiot, P.; Jarvis, M.; Nimlos, M.; Blanquart, G. Chemical kinetic modeling of tar formation during biomass gasification. In *2010 Spring Meeting of the Western States Section of the Combustion Institute, Boulder, Colorado*, 2010
(50) Van Poppel, B. P.; Desjardins, O.; Daily, J. W. *J. Comput. Phys.* **2010**, *229*, 7977−7996.
(51) Anca-Couce, A.; Sommersacher, P.; Scharler, R. *J. Anal. Appl. Pyrolysis* **2017**, *127*, 411−425.
(52) Chen, L. Fast pyrolysis of millimetric wood particles between 800 and 1000 °C. Ph.D. Thesis, Lyon I, Lyon, France, 2009.
(53) Park, W. C.; Atreya, A.; Baum, H. R. *Combust. Flame* **2010**, *157*, 481−494.
(54) Jia, L.; Le-Brech, Y.; Shrestha, B.; Frowein, M. B.-v.; Ehlert, S.; Mauviel, G.; Zimmermann, R.; Dufour, A. *Energy Fuels* **2015**, *29*, 7364−7374.

DOI: 10.1021/acs.energyfuels.7b01634
Energy Fuels 2017, 31, 12120−12132